Modifications in solvent clusters embedded along the fibers of a cellulose polymer network cause paper degradation

Marco De Spirito,[1,*] Mauro Missori,[1,2] Massimiliano Papi,[1] Giuseppe Maulucci,[1] Jose Teixeira,[3] Carlo Castellano,[4] and Giuseppe Arcovito[1]

[1]*Istituto di Fisica, Universitá Cattolica S. Cuore, L.go Francesco Vito 1 I-00168, Rome, Italy*

[2]*Istituto Centrale per la Patologia del Libro, Ministero per i Beni e le Attivitá Culturali, v. Milano 76, I-00184, Rome, Italy*

[3]*Laboratoire Léon Brillouin (CEA/CNRS), Saclay F-91191, Gif-sur-Yvette, France*

[4]*Dipartimento di Fisica, Universitá di Roma, "La Sapienza" P. le A. Moro, 2 I-00185, Rome, Italy*

(Received 6 November 2007; revised manuscript received 7 January 2008; published 1 April 2008)

Plants, algae, and their derivatives (paper, textiles, etc.) are complex systems that are chiefly composed of a web of cellulose fibers. The arrangement of solvents within the polymeric structure is of great importance since cellulose degradation is strongly influenced by water accessibility and external agents. In this paper we develop a model that is able to deconvolve the scattering contributions of both polymeric structures and solvent clusters trapped along the polymeric fibers. The surface morphology of cellulose fibers and the spatial distribution of water-filled pores and their dimensions have been recovered from small angle neutron scattering and atomic force microscopy data in function with paper degradation. In addition to providing a boost to the effort to preserve cellulose-supported material (included cultural heritage), the relevance of our model resides in the exploitation of a large number of biopolymer networks that are known to share structures similar to that of cellulose.

DOI: 10.1103/PhysRevE.77.041801 PACS number(s): 36.20.−r, 61.05.F−, 81.05.Lg

I. INTRODUCTION

Paper has been the most widely used writing support since the Middle Ages in the Western World [1,2] and even earlier in China and the Far East [3], due to the fact that one of the most abundant biomaterials present on Earth—cellulose—is the principal component used in its production [4]. Paper sheets represent a rather complex material primarily composed of a web of natural fibers of cellulose, with other substances, usually less than 5–10% in weight, being added depending on the production technique employed. In ancient times paper was produced from linen, hemp, and cotton cellulose obtained from rags and impregnated with a sizing material (i.e., gelatine), with fillers sometimes being added [5].

Cellulose is a composite (crystalline-amorphous) biomaterial possessing unique properties and outstanding stability. It is composed of a linear homopolysaccharide made up of repeating units of β-(1,4)-*D-glucopyranose*. The ability of the hydroxyl groups to form secondary valence hydrogen bonds with one another is the reason for the high tendency of cellulose polymers to organize themselves into parallel arrangements of crystallites and crystallite strands, the basic elements of the supermolecular structure of cellulose fibers (microfibrils), which in turn have been found to be composed of an assembly of crystalline domains and amorphous regions. In the case of flax and cotton, the crystalline domains have dimensions of ~5–6 nm in cross section and ~100 nm in length, while chains run parallel to the fiber axis, the fiber repeat is 1.03 nm corresponding to two glucose rings [4,6]. The cellulose fibers diameter ranges between 1–10 μm.

Paper's physical and chemical properties have been found to depend on its cellulose content chain length, on the degree of extension of the cellulose crystalline and amorphous zones, and on the presence of substances added during the fabrication process [7]. Cellulose degradation is caused by modifications in its organic groups as a result of reactions such as hydrolysis and oxidation, which occur upon natural or accelerated aging [4,8].

Hydrolysis and oxidation are enhanced by the presence of external agents, which, because they can only penetrate with difficulty the crystally\ine phase (on account of the strong interchain forces) principally affect the amorphous regions [4,9]. In the accessible (disordered) regions of cellulose all protons that are part of hydroxyl (OH) groups can be exchanged by deuterium in the course of a D_2O exchange process. Disordered regions can be localized within microfibrils (amorphous regions) and at the surface of microfibrils. The sorption of (heavy) water vapor by interaction with accessible hydroxyls in such disordered regions is the predominant process at relative humidities lower than 50–60%. Up to this level, as the accessible surfaces are covered with sorbed (heavy) water, it is assumed that (heavy) water is condensed by either capillary condensation in voids or pores, or by adsorption in multimolecular layers [4,9].

In relation to the above, nuclear magnetic resonance (NMR) experiments have revealed the presence of nanometric water aggregates in the cotton cellulose found in modern paper. The water domains permeate the amorphous regions of cellulose microfibrils in the form of fully confined pores of radius 1.4–1.5 nm [10].

Small angle neutron scattering (SANS) and small angle x-ray scattering have already been used to investigate the supramolecular structure of modern paper and cellulose fibers [11–14], but scattering data were only interpreted in terms of cellulose polymer network (microfibrils), without

*m.despirito@rm.unicatt.it

TABLE I. Details of the modern and ancient specimens measured in the experiment. PC1 values result from the PCA analysis of optical spectra of ancient samples, as described in the text. The state of degradation of ancient specimens increases by decreasing PC1 [19].

Sample label	Sample description	Fiber type	Aging or state of degradation	PC1 value
		Modern samples		
*F*6	Fabriano-Perusia, 1950	22% cotton/ 78% cotton linters	Unaged	
*W*0	Whatman No. 1, 2000	Cotton	Unaged	
*F*5	Fabriano-Perusia, 1950	22% cotton/ 78% cotton linters	Artificially aged	
*W*4	Whatman No. 1, 2000	Cotton	Artificially aged	
		Ancient samples		
*M*3	Milan, 1430	Cotton/linen	Good	14.13
*P*7	Perpignan, 1413	Linen	Intermediate	7.00
*M*2	Milan, 1430	Cotton/linen	Bad	4.96
*N*1	Nuremberg, 15th century	Linen	Very bad	−14.91

taking into account any possible contribution deriving from water confined in pores at mesoscopic length scales, as suggested by the NMR experiments. Recently, by using SANS, we have investigated the cellulose's supramolecular structure in ancient and modern samples [15]. SANS data were interpreted in terms of the superimposition of at least two contributions: (i) the expected scattering from the cellulose fibers' surfaces and (ii) the scattering from the distribution of water clusters confined to pores at a mesoscopic level, whose sizes increase approximately 1.5 to 2.0 nm, depending on the state of degradation. Because of the peculiar lengths scale separation occurring between the two phases we were able to analyze separately the low-q and the high-q segment of SANS spectra, hence the two scattering contributions were recovered. In a more general case where, instead, scattering contributions are superimposed, an analytical model to deconvolve scattering contributions is still required. This is no trivial matter since this is also the case in a number of biological systems in addition to cellulose, such as fibrin gels or amyloid fibers [16–18]. Therefore, in this paper we propose a model that predicts the scattering distribution of a polymer network with solvent clusters entrapped along the polymeric fibers. Moreover, we show that our model, applied to SANS or atomic force microscopy (AFM) data obtained from modern, artificially aged and ancient paper samples, provides details of the surface morphology of cellulose fibers, the spatial distribution of water-filled pores, and the increasing dimensions of water domains in cellulose which takes place in the course of degradation. Such detailed knowledge of cellulose fibers sheds light on the intimate structure of the elementary fibrils of cellulose and, possibly, will provide a boost to the effort to preserve paper-supported cultural heritage.

II. MATERIALS AND METHODS

A. Materials

The paper samples used in this work belong to three groups: modern samples, modern artificially aged samples, and ancient samples displaying increasing states of degradation. For the modern samples, chromatography grade pure cotton cellulose Whatman No.1 (labeled as *W*0 and *W*4) and Fabriano-Perusia (Fabriano Mill, Italy) papers (labeled as *F*5 and *F*6) were investigated (see Table I for more details). Artificial aging was performed in a climatic chamber for 28 days at 80 °C and 65% relative humidity (RH) in dark conditions, in accordance with ISO 5630–3:1986 standard. The aging conditions were chosen so as to produce an intermediate state of degradation between the unaged sample and the ancient sample originating from the best conservation conditions. Ancient specimens bearing no print (labeled as *N*1, *M*2, *M*3, and *P*7) consisted of small pieces of dated and identified paper, presenting various levels of degradation and discoloration, produced during the 15th century in European countries. The states of degradation of ancient specimens were classified by measuring the optical reflectance in the ultraviolet, visible and near infrared range followed by Principal Component Analysis of the measured spectra [19]. The peaks at 1663 and 1541 cm^{-1} of the amide I and II bands obtained through Fourier transform infrared spectroscopy confirmed that all the samples, with the exception of *W*0 and *W*4, were sized using gelatine, as was customary in ancient times in order to improve the paper's writing quality and surface characteristics [5,20].

B. SANS

Three sets of specimens were created by cutting three adjacent pieces (1×2.5 cm^2 each) from each paper sample. Since neutron waves incident on a material are scattered by variations (contrast) in the scattering length density of the medium, hydrogen-deuterium exchange from D_2O liquid or vapor phase was used in these experiments to modulate the scattering contrast [21]. When cellulose is exposed to D_2O vapors, the accessible hydroxyl groups in the previously described disordered regions readily exchange their hydrogen atoms for deuterium atoms, and a heavy water cluster forma-

tion phenomenon takes place [4,9,10]. The enhance contrast while minimizing the incoherent background signal and contextually avoiding the occurrence of relevant permanent deformation of cellulose polymers due to liquid H_2O or D_2O swelling the cellulose fibers, vapor phase exchange in a controlled climatic chamber have been employed. Indeed, over the 0–100% range of RH at room temperature, cellulosic materials expand up to approximately 1% (see Vol. 2, Chap. 3 of Ref. [7]).

Hydrated samples (H series) were left to equilibrate for at least 2 h in a glove-box (safe handling enclosure) containing an H_2O saturated atmosphere, and then sealed in closed sample holders with quartz windows. The time needed to reach water-paper equilibrium was tested in advance by using a gravimetric method, which showed that less than an hour is required. Fully deuterated (D series) and partially deuterated (HD series) samples were obtained in a two-step process: first the water content was eliminated by exposing the samples to a dry N_2 atmosphere for at least 2 h, then the samples were left to equilibrate for at least 2 h in a D_2O or in a $50\%H_2O/50\%D_2O$ mix saturated atmosphere. The samples were then sealed in sample holders with quartz windows.

Measurements were performed on the SANS Instrument D11 at Institut Laue-Langevin (ILL) in Grenoble, and on the PAXE beam line at Laboratoire Léon Brillouin, Saclay, France. In both cases scattering intensities were recorded by a two-dimensional position-sensitive detector. At D11 three different instrument settings were used corresponding to a momentum transfer range $q=4\pi/\lambda \sin(\vartheta/2)$ of $0.018<q<2.1$ nm^{-1}. Cell by cell spectra normalization was performed to account for the observed inhomogeneous intensity distribution. Cadmium measurements were performed in order to correct for the electronic background. At PAXE, two different instrument settings were used corresponding to $0.081<q<3.32$ nm^{-1}. Plexiglass was used for instrumental calibration. The differential scattering cross section per unit volume of the paper samples was calculated either by using the known wavelength dependent effective differential cross section of H_2O (ILL) or by measuring the absolute intensity of the incident beam (Saclay). In both cases data were also corrected for the dead time of each measurement [22,23]. Each sample's thickness (necessary for the calibration) was determined using a high-precision tool based on a magnetic gauge.

In order to analyze the scattered pattern let us recall that the neutron counts recorded within a solid angle $d\Omega$ in a detector pixel, in a time interval t, can be expressed as [24]

$$I(q) = KdT\frac{\partial\sigma}{\partial\Omega}(q), \tag{1}$$

where K is a constant instrumental factor, d is the sample thickness, and T is the sample transmission coefficient of the incident radiation. The differential cross section $\frac{\partial\sigma}{\partial\Omega}(q)$ per unit volume of a collection of interacting particles can be written as the product of a structure factor $S(q)$, which describes the spatial correlation between each particle's center-of-mass, and a form factor $P(q)$, which describes the internal structure of each particle

$$\frac{\partial\sigma}{\partial\Omega}(q) = N_P V_P^2 \Delta\delta^2 P(q) S(q), \tag{2}$$

where N_p is the number of particles per unit volume (N/V), V_p is the volume of the scattering particles, and $\Delta\delta^2$ is the square difference in neutron scattering length density (contrast). The form factor $P(q)$ and the structure factor $S(q)$ are dimensionless quantities given by

$$P(q) = \frac{\int_v h(r)e^{iqr}dr}{\int_v h(r)dr}, \tag{3}$$

$$S(q) = 1 + \frac{N}{V}\int_V [g(r)-1]e^{iqr}dr, \tag{4}$$

where $h(r)$ is the single particle density-density correlation function, $h(r)=\langle\rho(0)\rho(r)\rangle$ with ρ being the particle density, and $g(r)$ is the pair correlation function given by $g(r)=(\frac{V}{N})^2\frac{1}{V}\Sigma_{i\neq j}^{N}\delta(r+r_i-r_j)$, with r_i being the particles coordinated and N/V is the particle number density. $g(r)$ is such that $g(0)=0$ and $g(\infty)=1$. When the particles are not correlated $[g(r)=1]$, $S(q)=1$ for all q, and one arrives at the well-known result for a perfect gas, which may be a good approximation for dilute solutions [25]. Conversely, when the particles are correlated $[0<g(r)<1]$, $S(q=0)$ is always different than 1, and tends to 1 only asymptotically for q values much larger than the reciprocal of the length scales over which the particles are correlated.

Equation (1) shows that density fluctuations characterized by a length scale ζ make a contribution to the neutrons scattered at q values given by $q\sim 2\pi/\zeta$. Therefore by measuring the intensity of neutrons scattered within a range $[q_{\min}, q_{\max}]$, it is possible to probe length scales in the range $2\pi/q_{\max}<\zeta<2\pi/q_{\min}$, which correspond approximately to 1 nm $<\zeta<350$ nm, for our q range.

C. AFM

The same specimens used for SANS measurement were also subject to analysis by atomic force microscopy (AFM). During measurement taking samples were left to equilibrate at room temperature and RH conditions ($rH\approx 50\%$). Measurements were carried out by using an SP-Magic SX (Elbatech, Italy) AFM in the tapping operation mode [26]. The microscope probe consisted of a NSC16 ultrasharp silicon nitride cantilever from MikroMash Co. of nominal force constant $k=40$ N/m and a tip radius of 10 nm. By examining AFM images we can learn about sample topology on length scales ranging from a few nm up to the full size of the image (approximately 36 μm). Indeed we recovered images at different magnification by collecting several images (512 $\times$512 pixels) spanning sizes ranging from 1 to 36 μm.

Quantitative details of the sample surface such as the Hurst exponent (H), which account for the self similarity of

the surface, or the surface fractal dimension (D_s) of papers (i.e., surface roughness) [27] can be estimated. Indeed, when a generic signal, of a length L, can be likened to that generated from a stationary random process, the power spectrum density (PSD) is the Fourier transform of the autocorrelation function $R(\tau)$ of the signal [28]

$$\mathcal{I}_{\mathrm{PSD}} = \frac{1}{L}\int_0^L R(\tau)e^{2i\pi\omega\tau}d\tau. \tag{5}$$

According to the Wiener-Kintchine theorem, the PSD can be related to the mean square displacement $\sigma(L)$ [28]:

$$\sigma^2(L) = \int_{\omega_{\min}}^{\infty} \mathcal{I}_{\mathrm{PSD}}(\omega)d\omega. \tag{6}$$

For self-similar systems $\sigma(L) \sim L^H$, thus from Eq. (6)

$$\mathcal{I}_{\mathrm{PSD}}(\omega) \sim \omega^{-(d+2H)}, \tag{7}$$

where d is the embedding dimension. In the case of one-dimensional analysis (as when analyzing line profiles) $d=1$ and D_s can be determined from the exponent of Eq. (7) [29] as

$$D_s = \frac{7-(d+2H)}{2}. \tag{8}$$

Finally, we can directly compare AFM and SANS data [30]. Indeed, by comparing the Porod regime behavior of the scattered intensity $[I(q) \sim q^{-(6-D_s)}]$ and Eq. (8) we can determine that

$$I(q) \sim \sqrt{\mathcal{I}_{\mathrm{PSD}}/q^5}. \tag{9}$$

To increase the q range spanned we created a master curve by combining line averaged PSDs from images of different magnifications [31,32]. Single line analysis was performed to avoid spurious frequencies due to sample's shift eventually occurring in course of image acquisition (roughly 1024 s to scan 512×512 pixels). q values ranging from $\sim 310^{-4}$ nm^{-1} (at the largest scale probed ~ 36 μm) to ~ 3 nm^{-1} (at the smallest scale probed $\sim 1/512$ μm) are obtained.

III. MODELING OF INNER STRUCTURE OF PAPER

The inner structure of a sheet of paper looks like a random network of many thick fibers tangled together to form a very complex structure (Fig. 1). Cellulose fibers (such as flax or cotton), whose diameter can be as much as 10 μm, appear to be very inhomogeneous: some of them are long and straight, while others are bent; still others branch off, and their distribution in space does not appear to be uniform. The void spaces among the fibers are also inhomogeneous, and in some cases, can be very large, up to several tens of microns. Fibers moreover are composed of a collection of densely packed microfibrils. Lack of microfibrils packaging order create, along the axis of the fibers, small disordered regions of size ξ that are able to locally trap solvents in cavities of size R (Fig. 2). Depending on the physical-chemical treatments to which the paper is subjected, SEM and AFM images are very different and show markedly different network structures and morphologies [33].

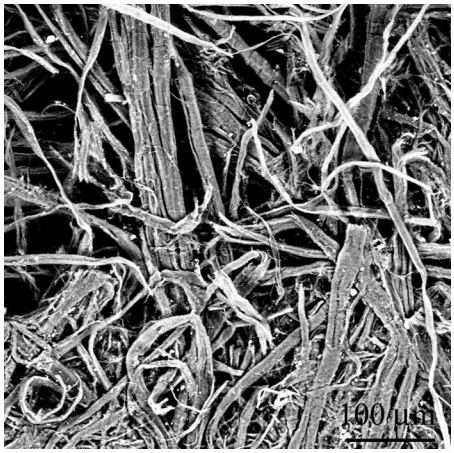

FIG. 1. Image of the sample $M3$, without prior preparation, has been obtained by using a Zeiss EVO40 variable pressure electron microscope. A random network of many thick fibers tangled together to form a complex structure can be observed. Fibers appear to be inhomogeneous; in addition, the diameters' size distribution does not appear to be uniform. The void spaces among the fibers are also inhomogeneous and, in some cases, can be very large, measuring up to several tens of microns.

Nevertheless, in spite of this large variety of possible scenarios, and based on the attractive features exhibited by the scattered intensity distribution (Fig. 5), a very simple model capable of describing the gel structure can be proposed. Let us imagine paper as a real two phase system: one is the cellulose polymer network [Fig. 2(a)], while the other is constituted by solvent clusters trapped in the amorphous regions [Fig. 2(c)].

In the case of a two phase system, scattering arising from the lack of homogeneity within the individual phases consists of three components [34]

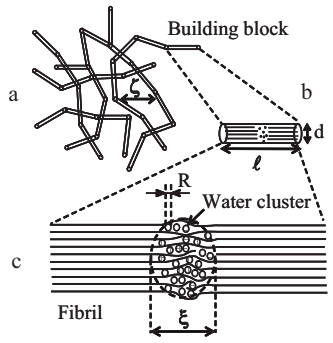

FIG. 2. Idealized structure of paper made out of cellulose fibers. The cellulose network, of mesh size ζ, is sketched as a collection of cylindrical segments bonded to each other (a), with an average diameter d and an average length ℓ (b). Each cylindrical segment, representing the cellulose fiber, is in turn composed of a collection of densely packed microfibrils. Small spherical clusters of radius R, representing trapped solvents, are localized in volumes of size ξ that are intercalated along the axis of the cylinder (c).

$$I(q) = I_1(q) + I_2(q) + I_{12}(q), \tag{10}$$

where $I_1(q)$ and $I_2(q)$ are the scattering contribution due to the density fluctuations present independently in the two phases and $I_{12}(q)$ represents the effects associated with the interaction of the waves scattered in the different phases [34]. Any correlation between the density fluctuations in the two phases across the phase boundaries is likely to be of short range, and consequently for small q, $I_{12}(q)$ is small and can be neglected. The intensity distribution scattered by a collection of interacting scatterers can be written as the product of a structure factor $S(q)$ and a form factor $P(q)$ [Eq. (2)]. In our case Eq. (10) can be expressed as

$$I(q) = A_1 S_1(q) P_1(q) + A_2 S_2(q) P_2(q) + B_{\text{inc}}, \tag{11}$$

where A_1 and A_2 are constants that depend on the number density of the scatterers and on the contrast between the solvent and the scatterers of phase 1 and 2 respectively, and B_{inc} is a q-independent scattering contribution essentially due to the incoherent cross section of hydrogen atoms [35].

To explain the contribution of the first phase, let us describe the cellulose fiber as an assembly of $n(n \gg 1)$ segments or "building blocks" which can be sketched as cylindrical segments with an average diameter d and an average length ℓ (Fig. 2). The segments are bonded together end-to-end, and at each bonding site, they can either be linked only to another segment, thus giving rise to linear chains, or branching off which produces a somewhat ramified structure (polymer network). Branched polymers may be described in terms of fractal theory [36] and since length scales probed by neutrons are much smaller than the size of cylindrical segments [15], the structure factor can be neglected [i.e., $S_1(q) = 1$] and the form factor of a collection of spatially correlated randomly oriented cylinders adopted [18].

$$P_1(q) = \left[\frac{1}{1 + (q\zeta)^2}\right]\left[\frac{1}{\left(1 + q^2\zeta^2\sqrt{\frac{\ell}{32d}}\right)^{\alpha/2}}\right], \tag{12}$$

where ζ is the polymer screening length (i.e., the network mesh size) and the exponent α depends on the surface fractal dimension (i.e., the surface roughness) [37].

The shape of solvent clusters trapped in amorphous regions of size ξ (i.e., the second phase) depends on pores morphology and on the local hydrophilic-hydrophobic character of pores internal surface [38]. Solvent clusters therefore have been likened to a collection of equivalent spheres of radius R distributed in the space with a mass fractal dimension d_f up to a distance ξ (Fig. 2), and the structure factor is [36]

$$S_2(q) = 1 + \frac{1}{(qR)^{(d_f)}}\frac{d_f\Gamma(d_f - 1)}{[1 + 1/q^2\xi^2]^{(d_f-1)/2}}\sin[(d_f - 1)\tan^{-1}(q\xi)], \tag{13}$$

where d_f, the sphere's distribution mass fractal dimension, is an index that characterize the local density. The sphere form factor instead can be written as

$$P_2(q) = \left[\frac{3[\sin(qR) - qR\cos(qR)]}{(qR)^3}\right]^2. \tag{14}$$

In conclusion, the overall scattered intensity can be expressed as

$$I(q) = A_1\left[\frac{1}{1 + (q\zeta)^2}\right]\left[\frac{1}{\left(1 + q^2\zeta^2\sqrt{\frac{\ell}{32d}}\right)^{\alpha/2}}\right] + A_2\left[1 + \frac{1}{(qR)^{(d_f)}}\frac{d_f\Gamma(d_f - 1)}{[1 + 1/q^2\xi^2]^{(d_f-1)/2}} \times \sin[(d_f - 1)\tan^{-1}(q\xi)]\right]\left[\frac{3[\sin(qR) - qR\cos(qR)]}{(qR)^3}\right]^2 + B_{\text{inc}}. \tag{15}$$

This is a general expression that describes the distribution of the scattering from a polymer network with solvent clusters trapped along polymeric fibers.

However, in the case that interests us, this expression can be simplified. Indeed cellulose fibers can posses diameters of as much as tens of microns, since the transferred momentum is much greater than the reciprocal of the fibers size $(qd \gg 1)$ and Eq. (12) reduced to the Porod law

$$P_1(q) = A_1 q^{-\alpha}. \tag{16}$$

In this case the overall fitting function became

$$I(q) = A_1 q^{-\alpha} + A_2\left[1 + \frac{1}{(qR)^{d_f}}\frac{d_f\Gamma(d_f - 1)}{[1 + 1/q^2\xi^2]^{(d_f-1)/2}} \times \sin[(d_f - 1)\tan^{-1}(q\xi)]\right]\left[\frac{3[\sin(qR) - qR\cos(qR)]}{(qR)^3}\right]^2 + B_{\text{inc}}. \tag{17}$$

Equation (17) therefore should allows us to capture all the structural features of cellulose fibers obtained from SANS spectra. In the attempting of a rapid recovery of R, a key parameter able to discriminate between differently aged papers (15), we plot simulated SANS spectra according to a classic Krakty plot [$I(q)q^2$ vs q]. As R increases, the peak intensity increases and the value of q at peak q^* shifts toward higher values of q [Fig. 3(a)]. Similarly the effect of R can be emphasized, on the shape of SANS spectra, by reporting [Fig. 3(b)] the product of $I(q)q^3$ in the q range used in the experiments. This choice of the axis has been made in order to enhance the spectral features at higher q where solvent clusters contribution is prominent. In both cases q^* appears directly proportional to R [see the inset of Fig. 3(b)] and by studying the slopes we found that $R = 1.70q^{*-1}$ (open square) for Krakty plot and $R = 2.27q^{*-1}$ (open circles) for the plot we suggest. The new plot therefore has to be considered as a useful alternative to the classic Krakty plot which, because of the better signal-to-noise ratio achievable, allows for an easier and safer determination of R.

IV. EXPERIMENTAL RESULTS

The scattering profile arising from a cellulose polymer network can be attributed to two phases: the cellulose poly-

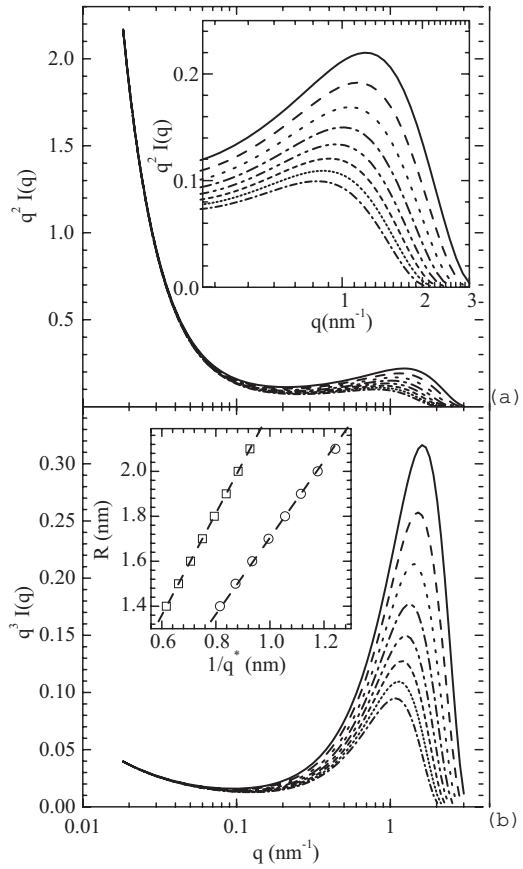

FIG. 3. The scattering intensity profiles, as simulated from the model Eq. (17), are reported according to the Krakty plot (a) or multiplied by q^3 (b). The parameters used in the simulation are A_1=0.00154, α=3.81, A_2=0.148, d_f=1.55, and ξ=20 nm, while R varies from 1.4 (dashed-dotted line) to 2.1 nm (continuous line) with 0.1 nm steps. Shown in the inset is the behavior of R in function with the inverse of the peak position in both cases (open square and open circles).

mers network, and the water or heavy water clusters trapped at a nanoscopic level in cellulose microfibrils [15]. To clarify the role played by solvent clusters we report, in Fig. 4, the intensity of the SANS profiles multiplied by q^3 for samples $M2_D$, $M2_H$, and $M2_{HD}$ (specifically, equilibrated in D_2O, H_2O, and 50%H_2O/50%D_2O saturated atmospheres, respectively). The three curves share a qualitatively similar shape with a well-distinguished peak at approximately 1.15 nm^{-1}, but of different amplitude (almost vanishing in the case of $M2_{HD}$). A simple analysis of the peak amplitude confirms a direct relation with the contrast. Indeed, the scattered intensity is proportional to the square of the scattering length density difference $(\Delta\rho)^2$. In our case we found $\frac{(\Delta\rho)^2_D}{(\Delta\rho)^2_H} \sim 3$ and $\frac{(\Delta\rho)^2_D}{(\Delta\rho)^2_{HD}} \sim 15$ to be values well in agreement with those expected (3.66 and 17.5, respectively). Therefore, since $M2_D$, $M2_H$, and $M2_{HD}$ spectra differ because of their H_2O or D_2O content we can attribute the peak to the constructive interference from a repeat structure produced by intercalation of water or heavy water as already proposed [10,15].

Therefore, since water or heavy water clusters, acting as powerful scatterers, provide a not negligible scattering contribution, whose intensity is proportional to the neutron scattering length density, we report the SANS profiles for all the samples of the D series where the best signal-to-noise ratio is achievable (Fig. 5). All the curves share a common behavior: a low-q decay followed by a roll off at higher q, which minutely, but continuously, shifts toward higher values of q with an increase in artificial or natural paper aging, suggesting its correlation to structural modifications induced by the degradation.

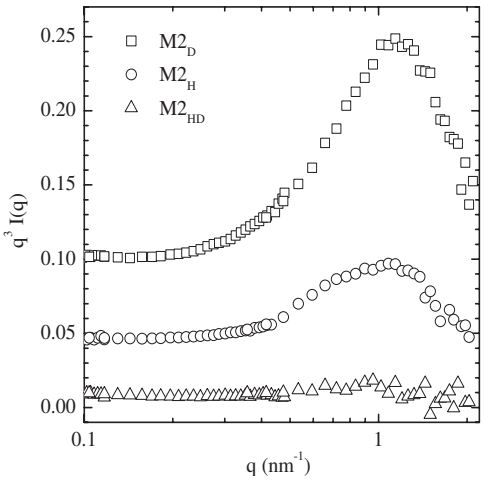

FIG. 4. Neutrons scattering intensities profiles subtracted from the incoherent background and multiplied by q^3 for samples $M2_D$, $M2_H$, and $M2_{HD}$. The peak at $\sim$1.15 nm^{-1} is very evident for $M2_D$ and $M2_H$ samples, while it almost disappears in case of sample $M2_{HD}$ sample.

Continuous lines in Fig. 5 represent the fit of Eq. (17) to SANS data. All the fitting parameters were left free to vary with the exception of ξ. Indeed in our samples the size of disordered regions within the cellulose fiber falls at length scales comparable with those spanned by fibers surface (of

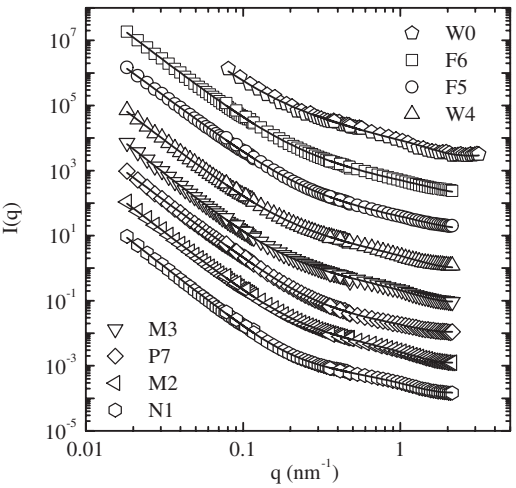

FIG. 5. Neutrons scattering intensities versus scattering vector q from all samples exposed to D_2O atmosphere (listed in Table I) are reported. Data are arbitrarily shifted for clarity. Best-fit curves are represented by continuous lines (see text for details).

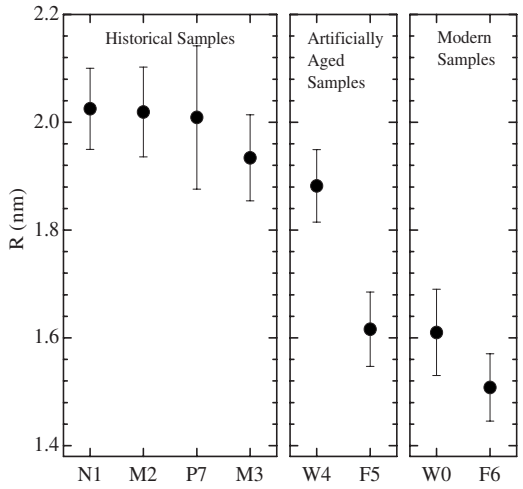

FIG. 6. The mean radius of the cluster is reported for all the samples investigated. Modern, artificially aged, and the ancient samples are plotted separately to make comparison easier. The cluster radius increases with the natural aging. The presence of a layer of coating (gelatin) on the fibers surface appears to protect against the increase of the cluster radius.

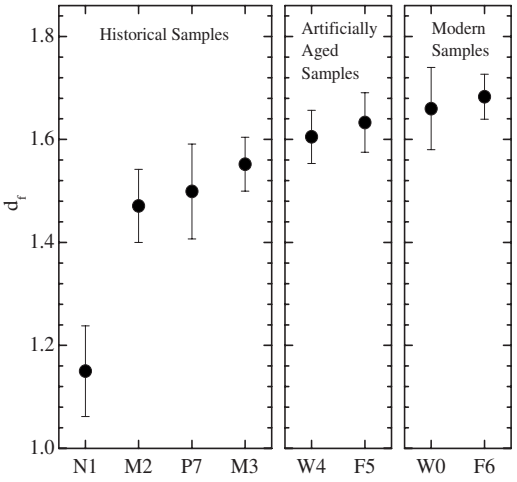

FIG. 7. The mass fractal dimension d_f for all samples exposed to the D_2O atmosphere is reported. The dependence of d_f on aging suggests that the solvent clusters within fibers rearrange their relative positions in a less compact structure.

much larger scattering contribution) and the fit appears insensitive of ξ. Therefore ξ has been fixed at 20 nm [4].

In Fig. 6 the clusters' radii of all samples are reported. In order to make comparison of our results easier, we have organized the samples into three classes: (a) modern samples (*F*6 and *W*0), (b) artificially aged samples (*W*4 and *F*5), and (c) the ancient samples (*N*1, *M*2, *M*3, and *P*7). Modern samples show a mean radius well in agreement with those already obtained from paper made of linters cellulose (conditioned at 50% *RH*) by NMR data ($R \approx 1.4-1.5$ nm) [10]. By artificially aging samples the mean radius increases. However, sample *F*5 has an *R* lower than that of sample *W*4 because of the protective effect of the collagen coating [15]. Naturally aged ancient samples, alternatively, shows a greater impact on *R* that appears larger than those of both modern and artificially aged samples, suggesting a higher degree of structural degradation of the polymers. Moreover, a clear dependence of *R* on aging up to a saturation value (~ 2 nm) is observed.

The spatial distribution of solvent clusters locally constrained along the cellulose fiber (amorphous regions) can be characterized by the volume fractal dimension d_f. Fractal dimensions (Fig. 7) of ancient samples (1.2–1.5) always appear lower than those of modern or artificially aged samples. This is compatible with solvent clusters arranged according an occasionally branched, pearl necklace structure pattern. In difference, less degraded samples (artificially aged or modern) have instead a larger d_f that approaches the values of 1.7 consistent with a more compact spatial distribution of such clusters.

The contribution to the SANS data arising from the cellulose polymer network, can be observed by looking at the slope of the low q part of the SANS spectra (α) [15]. Heavy water adsorbed in multimolecular layers at the microfibrils surface results in an increasing of a factor $\frac{(\Delta\rho)_D^2}{(\Delta\rho)_H^2} \sim 3$ of the parameter A_1 in case of deuterated samples with respect to samples equilibrated in H_2O. However, in our case α (data not shown) appears to be almost insensitive both to the modulation of the scattering contrast and to the state of degradation of the paper and can be averaged to 3.7 ± 0.1. This value of α is lower than that expected for sharp interfaces ($\alpha=4$) and indicate the presence of a rough surface characterized by a surface fractal dimension $D_s=6-\alpha$ that in our case is $D_s=2.3$

Finally representative AFM images of cellulose fibers from samples *F*6, *W*4, and *N*1 are reported in Fig. 8. As can clearly be seen, fibers appear, as expected, to be composed of an assembly of densely packed microfibrils, which bestow a certain degree of roughness. Roughness, quantified by the surface fractal dimension, can be recovered from AFM images by accounting for the power spectra density according to Eq. (8). In Fig. 8 we also report the intensities profiles as obtained from different scales (from 1 to 36 μm) AFM images analysis [Eq. (9)] together with SANS data for the three samples investigated. In all the samples SANS perfectly overlap AFM data in the low-q range, but shows a shoulder at higher q. Since the AFM technique is only sensitive to the cellulose fibrils' surface this result strongly supports the assignment of the shoulder of SANS data (i.e., the peak of Fig. 4) to water cluster aggregates embedded in the cellulose fibers (solvent clusters) and not to any structural part of cellulose fibers.

V. CONCLUSIONS

Polymer and biopolymer networks constitute a large class of systems which have for a considerable time been attracting the interest of scientists because they constitute good models for the physics of complexity, in addition to offering extremely wide applications in chemistry, biology, and the life sciences in general. Indeed, networks of biological molecules are of broad interest because they play fundamental roles (both physiological and pathological) in living entities. Actin and fibrin gels, and amyloidlike fibrillar aggregates,

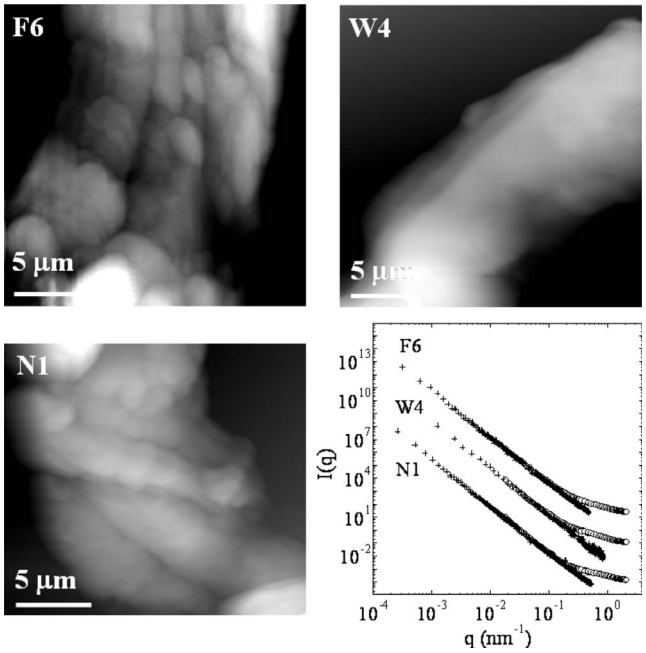

FIG. 8. Representative AFM images of *F*6, *W*4, and *N*1 samples are reported. Fibers appear to be composed of an assembly of densely packed protofibrils, which bestow a certain degree of roughness. The good agreement between neutrons scattering intensities profiles (open circles) and the intensities profiles, as obtained from different scales AFM images analysis (crosses), strongly supports the model we suggest and also allow for the calculation of the surface fractal dimension.

are just a few examples where the three-dimensional structure of their networks governs their biological functions [16–18].

In this context it is well understood [7] that the arrangement of solvents within the polymeric structure is of primary importance since they can modify the mechanical and physicochemical properties of the network. In this paper we have investigated paper, a complex material of great relevance both for its industrial applications and for its historical value; it is a material that is primarily composed of a web of fibers of cellulose, which are permeable to external solvent molecules.

Accessibility of water and external agents is in this case one of the main causes of cellulose degradation. Indeed, SANS and AFM data from a cellulose network show that solvents, although embedding in polymers' fibers, are trapped locally in small cavities, at a nanoscopic level, in between cellulose protofibrils. In relation to this, we have developed a model that which, while allowing for the recovery of structural details of the cellulose fibers, also constitutes a helpful tool to quantitatively assess levels of paper degradation.

Artificial and natural aging increase the water clusters' dimensions (R) up to a limiting values close to that of the protofibrils' radius. Accordingly, the spatial distribution of the solvent clusters, quantified by the fractal dimension d_f, while initially appearing to be randomly distributed in the space following a branched structure pattern along the cellulose fibers, modifies, tending toward linear arrangements (pearl-necklace structure). These results, moreover, provide a detailed insights into the currently accepted structural model of cellulose fibers of repetitive crystalline and amorphous phases.

The different modalities of water's accessibility to the inner structure of cellulose polymers are directly linked to the paper's state of degradation [15]. Indeed, as was customary in ancient times, the simple addition of gelatin, acting as a barrier and as a sacrificial layer, considerably reduces the macroscopic degradation caused by environmental agents [5,20]. Moreover, short time hydrothermal treatments (artificial aging), affecting both the cellulose's molecular structure [20] and the supramolecular arrangements of cellulose polymers, appear to be an accurate method for the simulation of overall natural aging, which is helpful for the validation of preservation and/or restoration treatments used on historical objects made of, or supported on, paper.

In conclusion, in addition to the fringe-micellar model classically adopted to describe the packaging of protofibrils in cellulose [4], we have proposed an alternative fractal model that allows for the recovery of available experimental data, allowing us to recover the surface morphology of cellulose fibers and the spatial distribution of the solvent-filled pores and their size. Such detailed knowledge of cellulose fibers sheds light on the intimate structure of the elementary fibrils of cellulose and, possibly, will provide a boost to the effort to preserve many different papers' historical properties. Finally, since similar structures are shared by a number of biological systems other than cellulose, our approach, which involves characterizing fibrillar networks at different length scales by combining imaging and scattering techniques, should be considered a not unimportant initiative which can be readily applied in other contexts.

ACKNOWLEDGMENTS

The authors wish to thanks Dr. F. Pinzari for providing paper electron microscope image and E. Muscianisi for his skilful technical assistance. This research was supported by COFIN Grant No. 2004054995 to M.D.S., by COFIN Grant No. 2005052299 to G.A., and by the Universitá Cattolica del Sacro Cuore, Roma, Italy.

[1] D. Hunter, *Papermaking. The History and Technique of an Ancient Craft* (Albert A. Knopf, London, 1957).
[2] V. Daniels, *The Paper Conservator* (Institute of Paper Conservation, Upton-upon-Severn, UK, 1988), Vol. 12, p. 93.
[3] R. Temple, *China, Land of Discovery and Invention* (Patrick Stevens, United Kingdom, 1986).
[4] H. Kraessig, *Cellulose. Structure, Accessibility and Reactivity*, Vol. 11 of Polymer Monographs (Gordon and Breach Science, Singapore, 1993).
[5] G. Righini, A. L. Segre, G. Mattogno, C. Federici, and P. F. Munafo, Naturwissenschaften **85**, 171 (1998).
[6] A. C. O'Sullivan, Cellulose **4**, 173 (1997).
[7] R. E. Mark, C. C. Habeger, Jr., J. Borch, and M. B. Lyne, *Handbook of Physical Testing of Paper* (Marcel Dekker, New York, 2002), Vols. 1,2.
[8] D. Klemm, H.-P. Schmauder, and T. Heinze, in *Polyasaccarides II Polysaccharides from Eukaryotes*, edited by A. S. S. De Baets and E. J. Vandamme (Wiley-VCH, Weinheim, 2003), Vol. 6, pp. 275–319.
[9] M. Müller, C. Czihak, H. Schober, Y. Nishiyama, and G. Vogl, Macromolecules **33**, 1834 (2000).
[10] D. Capitani, N. Proietti, F. Ziarelli, and A. L. Segre, Macromolecules **35**, 5536 (2002).
[11] A. Guinier and G. Fournet, *Small-Angle Scattering of X-rays* (John Wiley and Sons, New York, 1955).
[12] E. W. Fischer, P. Herschenroeder, R. S. J. Manley, and M. Stamm, Macromolecules **11**, 213 (1978).
[13] C. J. Garvey, I. H. Parker, R. B. Knott, and G. P. Simon, Holzforschung **58**, 473 (2004).
[14] M. Müller, C. Czihak, G. Vogl, P. Fratzl, H. Schober, and C. Riekel, Macromolecules **31**, 3953 (1998).
[15] M. Missori, C. Mondelli, M. De Spirito, C. Castellano, M. Bicchieri, R. Schweins, G. Arcovito, M. Papi, and A. C. Castellano, Phys. Rev. Lett. **97**, 238001 (2006).
[16] C. Dobson, Philos. Trans. R. Soc. London, Ser. B **356**, 133 (2001).
[17] M. A. Dichtl and E. Sackmann, Proc. Natl. Acad. Sci. U.S.A. **99**, 6533 (2002).
[18] F. Ferri, M. Greco, G. Arcovito, F. A. Bassi, M. De Spirito, E. Paganini, and M. Rocco, Phys. Rev. E **63**, 031401 (2001).
[19] M. Missori, M. Righini, and S. Selci, Opt. Commun. **231**, 99 (2004).
[20] M. Missori, M. Righini, and A.-L. Dupont, Opt. Commun. **263**, 289 (2006).
[21] J. Higgins and H. Benoit, *Polymers and Neutron Scattering* (Clarendon Press, Oxford, 1994).
[22] P. Lindner and T. Zemb, *Neutron, X-rays and Light. Scattering Methods Applied to Soft Condensed Matter* (North Holland, Amsterdam, 2002).
[23] J. Teixeira, in *Structure and Dynamics of Supramolecular Aggregates and Strongly Interacting Colloids*, edited by S.-H. Chen, J. Huang, and P. Tartaglia (Kluwer, Dordrecht, 1992).
[24] R.-J. Roe, *Methods of X-Ray and Neutron Scattering in Polymer Science* (Oxford University Press, Oxford, 2000).
[25] M. Kerker, *The Scattering of Light and Other Electromagnetic Radiation* (Academic Press, New York, 1969).
[26] M. Papi, G. Arcovito, M. D. Spirito, M. Vassalli, and B. Tiribilli, Appl. Phys. Lett. **88**, 194102 (2006).
[27] W. Zahn and A. Zösch, Fresenius J. Anal. Chem. **358**, 119 (1997).
[28] R. M. Howard, *Principles of Random Signal Analysis and Low Noise Design* (John Wiley and Sons, Hoboken, NJ, 2002).
[29] R. Voss, in *Scaling Phenomena in Disordered Systems*, edited by R. Pynn and A. Skyeltorp (Plenum, New York, 1985).
[30] J. Erlebacher, M. J. Aziz, E. Chason, M. B. Sinclair, and J. A. Floro, Phys. Rev. Lett. **82**, 2330 (1999).
[31] J. Gutmann, P. Muller-Buschbaum, and M. Stamm, Faraday Disc. **112**, 285 (1999).
[32] P. Muller-Buschbaum, J. Gutmann, and M. Stamm, Phys. Chem. Chem. Phys. **1**, 3857 (1999).
[33] H. Zhao, J. Kwak, Z. Zhang, H. Brown, B. Arey, and J. Holladay, Carbohydrate Polymers **68**, 235 (2007).
[34] H. Bale and P. Schmidt, Phys. Rev. Lett. **53**, 596 (1984).
[35] J. Fitter, T. Gutberlet, and J. Katsaras, *Neutron Scattering in Biology: Techniques And Applications* (Springer, Berlin, 2006).
[36] J. Teixeira, J. Appl. Crystallogr. **21**, 781 (1988).
[37] S. K. Sinha, T. Freltoft, and J. Kjems, in *Kinetics of Aggregation and Gelation*, edited by F. Family and D. Landau (North Holland, Amsterdam, 1984), p. 87.
[38] L. Brovchenko, A. Geiger, A. Oleinikova, and D. Paschek, Eur. Phys. J. E **12**, 69 (2003).